IEEE Access
Multidisciplinary | Rapid Review | Open Access Journal

Received August 12, 2017, accepted August 27, 2017, date of publication August 30, 2017, date of current version September 27, 2017.

Digital Object Identifier 10.1109/ACCESS.2017.2746800

Ka-Band Linear to Circular Polarization Converter Based on Multilayer Slab With Broadband Performance

MOHAMMAD AKBARI[1], (Student Member, IEEE), MOHAMMADMAHDI FARAHANI[2], (Student Member, IEEE), ABDEL-RAZIK SEBAK[1], (Fellow, IEEE), AND TAYEB A. DENIDNI[2], (Senior Member, IEEE)

[1]Department of Electrical and Computer Engineering, Concordia University, Montreal, QC H3G2W1, Canada
[2]Institut National De La Recherche Scientifique, Montreal, QC H5A1C6, Canada

Corresponding author: Mohammad Akbari (akbari.telecom@gmail.com)

ABSTRACT In this paper, a Ka-band polarization converter is presented, which is based on multilayer slab. In order to improve impedance matching, metallic circular traces are printed periodically on each dielectric multilayer slab. Simulated results of the polarizer show that it can transform linearly polarized (LP) to circularly polarized (CP) fields over a frequency band from 23 to 35GHz (42%) with an insertion loss less than 0.5 dB. The transmitted CP wave by the polarizer is approximately robust under oblique illuminations. The polarizer is fabricated and measured by a wideband horn antenna satisfying the simulated results. Next, in order to design a high-gain CP structure around 30 GHz, an 8-element LP array antenna with Chebyshev tapered distribution is designed and integrated with the polarizer. Obviously, the antenna limits the overall bandwidth (nearly 28 to 31.5 GHz) due to the narrowband nature of the LP antenna array. When the polarizer is illuminated by an incident LP wave, the two linear components of the transmitted wave with approximately equal amplitudes and 90° phase difference on the frequency band of interest are produced. Experimental results of the proposed structure show a pure CP with a gain of 13 dBi at 30 GHz, which can be suitable for millimeter wave communication.

INDEX TERMS Polarizer, Ka-band, linear, circular, polarization converter, dielectric multilayer.

I. INTRODUCTION

Polarization properties of antennas play a critical role in wireless communication systems. Recently, because of the advanced signal propagation properties, systems using CP antennas offer significant performance benefits over systems using traditional linearly polarized antennas. The use of CP is considered as a solution for addressing challenges associated with adverse weather conditions, and polarization mismatch, none-line-of- sight applications, phasing issues, and multipath effects [1]–[3]. Various CP antennas have been presented in the literature in the last few decades. A suitable way of creating a CP wave is to radiate a linearly polarized electromagnetic wave to a polarizer plane. This method has become appealing in situations where the radiating structure contains a planar array. For this case, the polarizer is placed on top of the antenna to transmit CP waves. Basically, the polarization converter decomposes the LP incident plane wave into two orthogonal components of nearly equal amplitude with a phase difference of 90° to generate a CP transmitted plane wave. A transmission-type polarization converters, which are also named polarizers, have been extensively investigated by researchers in the open literature for several applications [4]–[13]. For example, some polarizers were designed utilizing frequency-selective surface (FSS) structures [4]–[7], and others are based on traditional hybrid meander line and loop configuration [8]–[10]. In [4] a multilayer FSS was designed using square patches with truncated corners to obtain 90° phase difference between orthogonal linear components. The polarizer presented in [5] employs a miniaturized-element FSS composed of arrays of subwavelength capacitive patches and inductive wire grids separated by dielectric substrates. The polarizer in [6] uses a double-sided partially reflective surface (PRS), which controls independently the reflection and transmission coefficients. The work in [7] suggested a CP converter utilizing a four layer FSS consists of split rings

bisected by a metal strip, in which distance between different layers is a quarter wavelength, but the layers' dimensions are different. Although structures suggested in [4]–[7] are broad band, they consist of multilayer structures with different configurations and dimensions for each layer, ending up with complicated geometry and configuration for the polarizers. In [9] single layer polarizer based on hybrid meander line and loop geometry are proposed. This structure can cover the AR bandwidth of 46.8%. However, the peak insertion loss is 3dB. In order to achieve a CP in [10], a meander line polarizer has been employed with the linear SIW antenna, while the structure does not have broadband behavior. Another approach used in [11] included rotating FSS structure that was implemented using the substrate integrated waveguide (SIW) technology. The rotating FSS in [12] utilizing a triple-mode SIW cavity resonator resulted in improving the transmission bandwidth. Meta-surface and metamaterial have been applied in [12]–[13]. A meta-surface of 16 rectangular loop unit cells each with a diagonal microstrip line is positioned above a source antenna in [12]. An ultra-compact chiral metamaterial (CMM) using triple-layer twisted split-ring resonators (TSRRs) structure was suggested in [13]. Despite the benefits proposed by these designs, the majority of them employ resonant elements that tend to be narrowband. In this study, a Ka-band transmission–type polarizer based on multilayer dielectric structure to convert LP incident electromagnetic wave into a CP transmitted wave is proposed. To simplify the structure, a unit cell is used in all dielectric layers. In order to illuminate the polarizer, an 8-element linearly polarized linear array antenna with Chebyshev tapered distribution to control the radiated pattern side lobe level (SLL) is also designed. In the configuration, the antenna is placed at a half free space wavelength from the polarizer with a 45° rotation. The size of the polarizer is determined using a diffraction and transmission rays' model. The benefits of the proposed structure include (a) wideband polarizer with high CP purity, (b) polarizer can function for broad-angle oblique incident waves, (c) less insertion loss, (d) simple structure using same unit cell in all layers, (e) employing a low SLL linear array antenna, and (f) implementation at mm-wave Ka-band. The proposed polarizer is based on a nano-polarizer with periodic and two-dimensional dielectric high-contrast gratings [14]. The basic theory and operation of the polarizer are discussed in Section II. Section III outlines the design process of the polarizer's unit cell. Simulated results of the proposed polarizer are presented and discussed in Section IV. The design of single and 8-element linear array antenna with Chebyshev tapered distribution are described in Section V. Section VI presents the measured results of the combined structure of the antenna and polarizer. Finally, a brief conclusion is given in Section VII.

II. THEORETICAL ANALYSIS

In this section, we consider the theoretical analysis of the polarizer. Fig. 1 exhibits the topology of the polarizer which converts linearly polarized EM wave into a circular one.

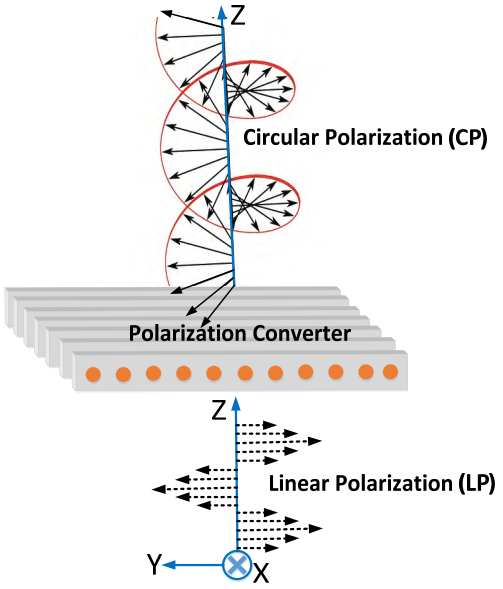

FIGURE 1. Schematic model of a linear-to-circular polarizer.

Let us consider an incoming plane wave that propagates in the +z direction, whose incident and transmitted electric fields can be expressed as [15]

$$E^{inc}(x, y, z, t) = \begin{pmatrix} E_x^{inc} \\ E_y^{inc} \end{pmatrix} e^{i(kz-t)} \tag{1}$$

Where ω, k, E_x, and E_y are the frequency, wave number, and the complex amplitudes of x- and y- electric field components, respectively [29].

$$E^{tr}(x, y, z, t) = \begin{pmatrix} E_x^{tr} \\ E_y^{tr} \end{pmatrix} e^{i(kz-t)} \tag{2}$$

To better understand the polarization conversion of the polarizer, the transmission coefficient T.C. is defined as:

$$T.C. = \frac{E^{tr}}{E^{inc}} \tag{3}$$

The linear transmission matrix can be expressed as [29]

$$\begin{pmatrix} E_x^{tr} \\ E_y^{tr} \end{pmatrix} = (T.C.)_{Linear} \begin{pmatrix} E_x^{inc} \\ E_y^{inc} \end{pmatrix} = \begin{pmatrix} T_{XX} & T_{XY} \\ T_{YX} & T_{YY} \end{pmatrix} \begin{pmatrix} E_x^{inc} \\ E_y^{inc} \end{pmatrix} \tag{4}$$

Thus, the circularly polarized transmitted EM wave can be defined as [29]:

$$\begin{pmatrix} E_{RHCP}^{tr} \\ E_{LHCP}^{tr} \end{pmatrix} = \begin{pmatrix} E_x^{tr} + jE_y^{tr} \\ E_x^{tr} - jE_y^{tr} \end{pmatrix} = (T.C.)_{Circular} \begin{pmatrix} E_x^{inc} \\ E_y^{inc} \end{pmatrix} \tag{5}$$

$$\begin{aligned} (T.C.)_{Circular} &= \begin{pmatrix} T_{RHCP\_X} & T_{RHCP\_Y} \\ T_{LHCP\_X} & T_{LHCP\_Y} \end{pmatrix} \\ &= \frac{1}{\sqrt{2}} \begin{pmatrix} T_{XX} + jT_{YX} & T_{XY} + jT_{YY} \\ T_{XX} - jT_{YX} & T_{XY} - jT_{YY} \end{pmatrix} \end{aligned} \tag{6}$$

where the factor $\frac{1}{\sqrt{2}}$ in (6) is due to power normalization. The matrix in (6) states the ability of the polarizer to convert an LP electromagnetic wave into a CP one. For the proposed structure, the cross transmission coefficients are considered to be negligible ($T_{YX} \approx T_{XY} \approx 0$). Therefore, we have

$$E^t_{RHCP} = \frac{1}{\sqrt{2}}\left[(T_{XX})\,E^{inc}_x + (jT_{YY})\,E^{inc}_y\right] \tag{7}$$

$$E^t_{LHCP} = \frac{1}{\sqrt{2}}\left[(T_{XX})\,E^{inc}_x - (jT_{YY})\,E^{inc}_y\right] \tag{8}$$

In order to generate a CP wave within a desirable frequency band, the following requirements should be satisfied.

$$|T_{xx}| = |T_{yy}| \tag{9}$$

$$\Delta\emptyset = \emptyset_{xx} - \emptyset_{yy} = \pm\frac{\pi}{2} \tag{10}$$

In (10), $+\frac{\pi}{2}$ corresponds to a RHCP transmitted wave, while $-\frac{\pi}{2}$ represents a LHCP one. The axial ratio (AR) of the polarizer is evaluated utilizing transmission line theory [16]:

$$AR = \left(\frac{|T_{xx}|^2 + |T_{yy}|^2 + \sqrt{a}}{|T_{xx}|^2 + |T_{yy}|^2 - \sqrt{a}}\right)^{\frac{1}{2}} \tag{11}$$

Where

$$a = |T_{xx}|^4 + |T_{yy}|^4 + 2\,|T_{xx}|^2\,|T_{yy}|^2 \cos(2\Delta\emptyset) \tag{12}$$

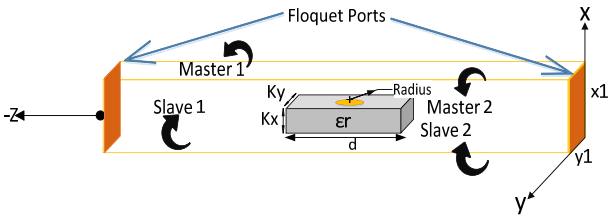

FIGURE 2. The unit cell model by HFSS software (x_1 = 1.6mm, y_1 = 1mm, d=4.6mm, kx=0.254mm, ky=1mm, εr=10.2, Radius=0.3mm).

III. POLARIZER DESIGN

The schematic model of the proposed multilayer dielectric LP to CP polarizer is shown in Fig. 1. The polarizer is illuminated by a planar LP electromagnetic wave propagating in the k direction and tilted away from the x-axis by 45°. Therefore, the electric field is decomposed into two orthogonal components: the former along the x-axis and the latter along the y-axis. Fig. 2 exhibits the unit cell model simulated by ANSYS HFSS^{TM}. The unit cell consists of two Floquet ports in distance of one wavelength (λ) far from the dielectric with constant ε_r = 10.2 and thickness k_x = 0.254mm. The width and length of the dielectric piece are ky=1mm and d=4.6mm, respectively. The radius of the metal circle is 0.3mm. In addition, the method applied in the unit cell model is the periodic boundary conditions of the Master/Slave in order to evaluate the infinite structure. Both Floquet ports contain two dominant modes with two orthogonal waves along x- and y-axis. The main idea of the LP-to-CP

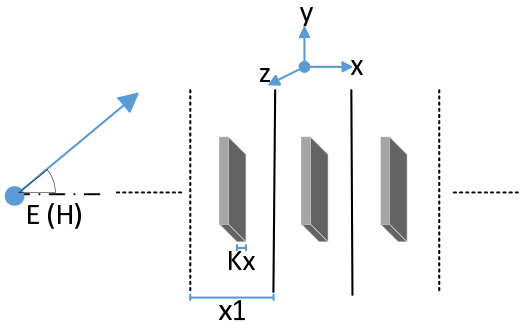

FIGURE 3. One dimensional lattice of dielectric slabs of width kx in a periodic lattice with period x_1.

polarizer and simulation model have come from [14], [17], and [18]. In order to study a fundamental theory for multilayer dielectric slabs, Fig. 3 is presented. A representative one-dimensional periodic array of dielectric slabs with period x_1 and dielectric insert width K_x is depicted in Fig. 3. If the electric field does not have a component in the x –direction, the mode is denoted TE_x or horizontal. If the magnetic field does not have a component in the x -direction, the mode is denoted TM_x or vertical.

The effective dielectric constants given in two directions by the volumetric average of the constitutive phases are [19], [20].

$$\varepsilon_{rx} = \begin{cases} \varepsilon_r, & -\frac{k_x}{2} < x \frac{k_x}{2} \\ 1, & otherwise.; \end{cases} \tag{13}$$

$$\varepsilon_{ry} = [1 + (\varepsilon_r - 1)\,\frac{k_x}{x_1}] \tag{14}$$

From (13) and (14) it can be noted that the effective dielectric constant in y-direction depends on $\frac{k_x}{X_1}$, while the x-directed component has a constant value close to 1. Therefore, due to the existence of the periodic dielectric slabs, a phase difference happens between the E-field orthogonal components when the incident EM wave transmits through the LP-to-CP polarizer. The phase difference is estimated as:

$$\text{Phase Difference} = (\beta_y - \beta_x)d = \frac{2\pi}{\lambda}(\sqrt{\varepsilon}_{ry} - \sqrt{\varepsilon}_{rx})d \tag{15}$$

where λ, β are the wavelength and phase constant, respectively. The phase difference between the E-field orthogonal components is tuned using a length parameter d, as shown in Fig. 2. In order to satisfy the CP requirement in (15), the phase difference must be $\frac{\pi}{2}$, therefore

$$d = \frac{\lambda_0}{4\left(\sqrt{\varepsilon}_{ry} - \sqrt{\varepsilon}_{rx}\right)} \tag{16}$$

The dielectric multilayer slab characteristics at a resonant frequency (f_r) are governed by (13) through (16), in which ε_{rx} can be estimated to 1. Thus, at 30 GHz with dielectric constant 10.2, thickness kx=0.254mm, and the periodic distance between slabs x_1 = 1.6mm, d=4.6mm is obtained.

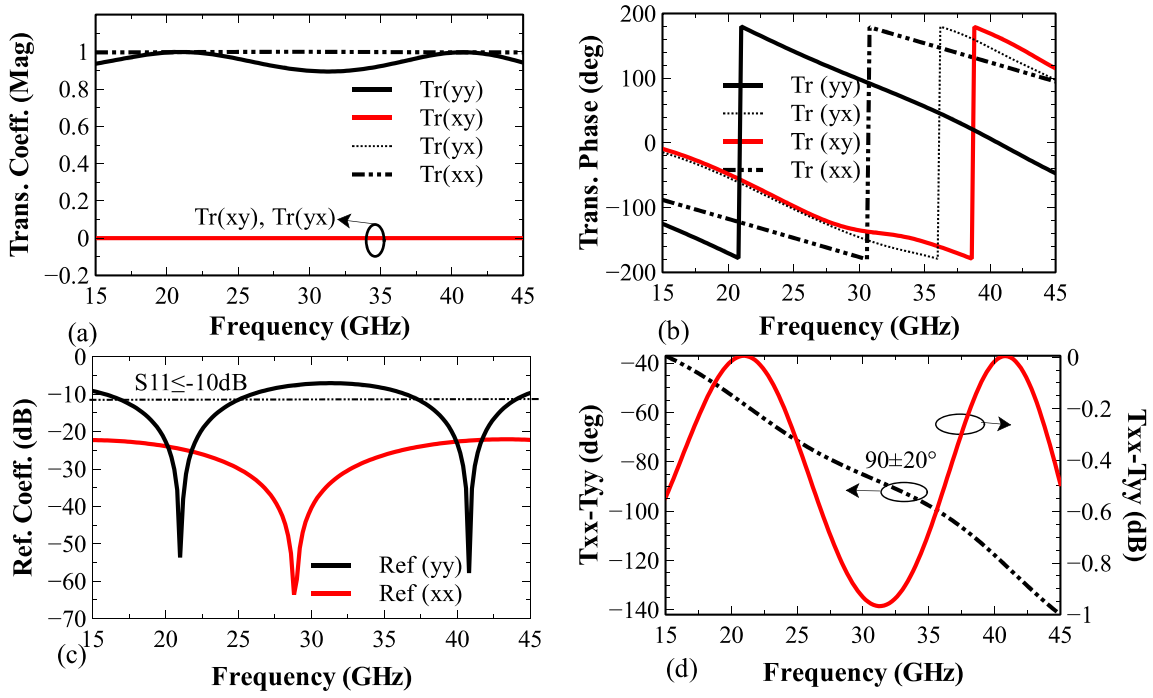

FIGURE 4. The simulated of transmission coefficients of dielectric slab without the conductor in unit cell model (a) magnitude of transmission coefficients, (b) phase of transmission coefficients, (c) reflection coefficient, and (d) difference of phase and magnitude between transmission coefficients.

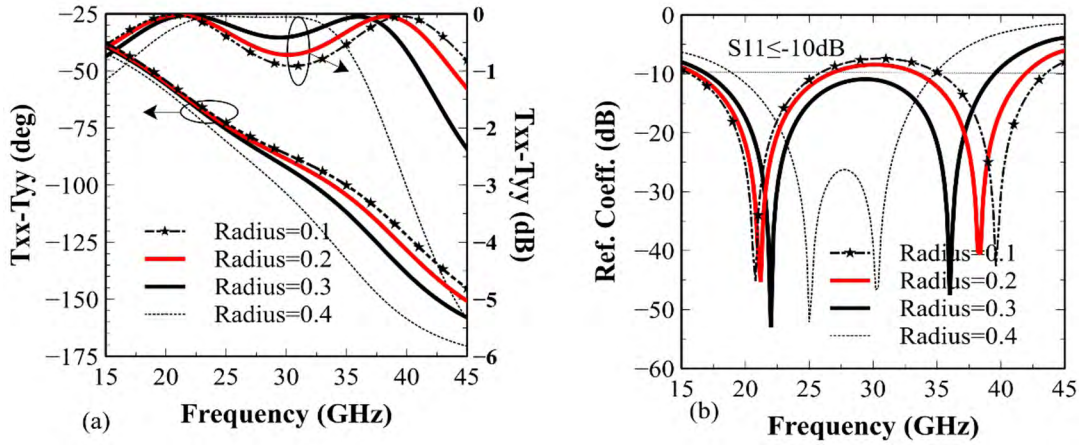

FIGURE 5. (a) variations of transmission coefficients and (b) reflection coefficients in the unit cell model when radius of the circle conductor changes.

IV. SIMULATION RESULTS OF POLARIZER

A. REFLECTION AND TRANSMISSION COEFFICIENTS

In order to investigate and verify the polarizer performance, a full-wave simulation is carried out using Ansys HFSS-15. Initially, the dielectric multilayer slabs with numerical values obtained from (13) to (16) are simulated. The magnitude and phase of transmission coefficients are presented in Fig. 4 (a) and (b), respectively. It can be noticed that the cross transmission coefficients Tr(xy) and Tr(yx) are nearly zero. Concerning the reflection coefficient curve depicted in Fig. 4 (c), there are two resonant frequencies at about 21GHz and 41GHz. Fig. 4(d) shows the magnitude and phase differences between transmission coefficients for both polarizations (xx and yy). It is observed that the phase difference (90±20°) and magnitude difference (less than 1dB) of transmission coefficients for both polarizations remain between 24GHz to 38GHz (45%). In terms of design simplicity without any conductors, the dielectric multilayer slabs can be a good polarizer candidate. However, the −10 dB impedance bandwidth is very limited. In order to satisfy the standard impedance bandwidth ($S_{11} \leq -10$dB), a circular conductor, due to its shape simplicity, is printed on one side of

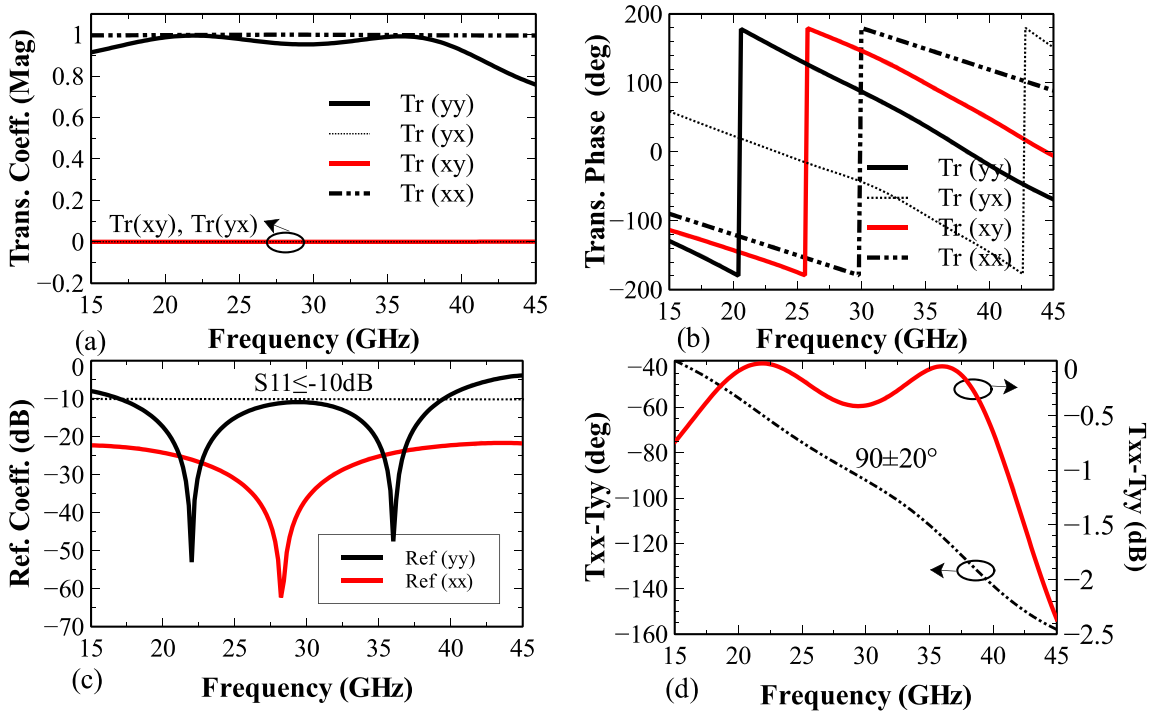

FIGURE 6. The simulated of transmission coefficients of dielectric slab with the conductor in unit cell model (a) magnitude of transmission coefficients, (b) phase of transmission coefficients, (c) reflection coefficient, and (d) difference of phase and magnitude between transmission coefficients.

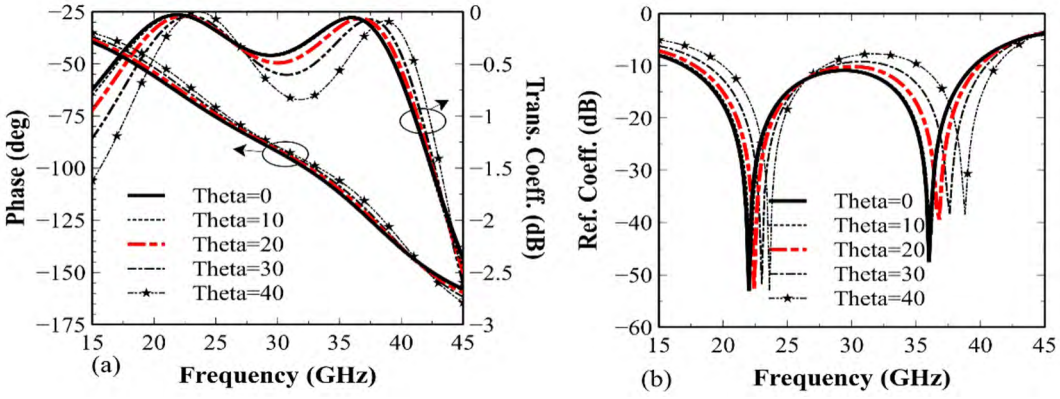

FIGURE 7. The results related to the dielectric slab with circle conductor in the unit cell model when is illumintated by an incident wave with different oblique angles (a) magnitude and phase of transmission coefficients, (b) reflection coefficients.

each dielectric slab. The circular conductor gives the designer freedom to achieve the desirable impedance bandwidth. The dependence of transmission and reflection coefficients of the dielectric slab on the radius of the integrated circular conductor are given in Fig. 5. A conducting circle with radius 0.3mm is chosen as a reasonable value.

Finally, the simulated transmission and reflection coefficients of the proposed polarizer with the conductor in the unit cell model are depicted in Fig. 6. It is obvious that the dielectric slab with a circular conductor has the same behavior in transmission coefficient curves in comparison with the dielectric slab without the conducting circle. The main improvement is observed in the bandwidth of reflection coefficient ($S_{11} \leq -10$dB), where it covers the frequency band 22.5GHz to 40GHz (56%). However, the phase difference of transmission coefficients (90±20°) limits the frequency band from 23GHz to 35GHz (42%). All obtained results are based on normal incident EM wave when the LP wave is titled away from the x-axis by 45°. Practically, the incident wave can be oblique or deflected due to the type of radiation pattern of antenna or installation inaccuracy. Therefore, the robustness of the polarizer under oblique incidence wave must be examined as well. As illustrated in Fig. 7, it is observed that the broad −10dB impedance bandwidth is still maintained up to

an oblique angle of 30°. It is also found out that by varying the incident wave angle, the transmission performance is approximately stable.

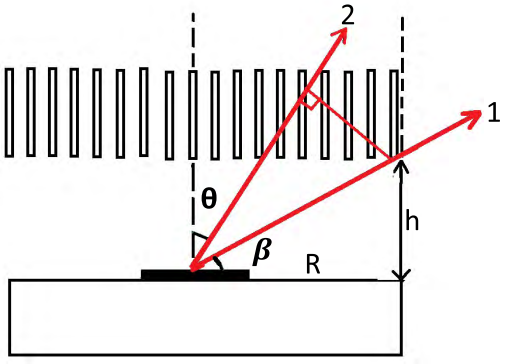

FIGURE 8. Model of the diffraction and transmission rays [2].

B. DIELECTRIC MULTILAYER SLABS ARRANGEMENT

One of the challenges in designing multilayer structures as superstrate (placed above the radiating sources) is to specify the number of layers and estimate the size of the superstrate. To address this challenge, the model of diffraction and transmission ray is shown in Fig. 8 [2]. This technique is useful for circular layers, but it can also give a good estimation for square shape layers. In this model, the phase of diffraction and transmission rays radiated from the antenna source to dielectric multilayer slabs should be equal.

In Fig. 8, rays 1 and 2 are the first diffraction and transmission with phases 1 and 2, respectively. Since the wave phase is defined as

$$\emptyset = e^{-j(\beta d)} = e^{-j(\frac{2\pi\sqrt{\varepsilon_r}}{\lambda_0}.d)} \tag{17}$$

Therefore, with respect to Fig. 8, we have

$$(\varphi)_1 = e^{-j(\frac{2\pi h}{\lambda sin\beta})} \tag{18}$$

$$(\varphi)_2 = e^{-j(\frac{2\pi h\cos(\frac{\pi}{2}-\beta-\theta)}{\lambda sin\beta}+(\phi_t))} \tag{19}$$

In order to keep the diffraction and transmission rays in phase, we impose the following conditions,

$$\frac{2\pi h}{\lambda sin\beta} = \frac{2\pi h\cos\left(\frac{\pi}{2}-\beta-\theta\right)}{\lambda\sin\beta} + (\phi_t) \tag{20}$$

$$\frac{h}{\lambda}\left(\frac{1}{sin\beta}-1\right) - \frac{(\phi_t)}{2\pi} = N \tag{21}$$

The proposed polarizer involves the transmission phase ϕ_t in x- and y- polarization, which are 179.7° and 87.5°, respectively. In order to have the minimum size of the polarizer, "N" should be a positive integer. The elevation angle β from the antenna source to the edge of the polarizer, for the two aforementioned directions, is computed as 15° and 17°, respectively, resulting in an ellipse with major and minor axes of 37mm and 33.4mm. Based on the diffraction and transmission rays' model, the size of the proposed dielectric slab as exhibited in Fig. 2 is 33×25 unit cells. It means that the proposed polarizer consists of 33 circular conductors which are linearly printed on each of the 25 dielectric layers.

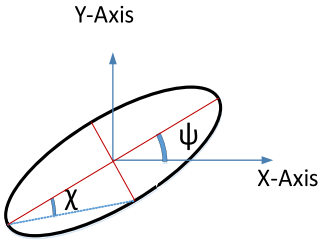

FIGURE 9. The polarization ellipse with two angles shown ψ and χ as the geometrical parameters of the ellipse.

C. POSITION OF THE TRANSMITTED WAVE POLARIZATION

In order to investigate the purity of transmitted wave CP, the polarization azimuth angle ψ, and ellipticity angle χ are used to examine the orientation and case of the elliptical polarization, as shown in Fig. 9.

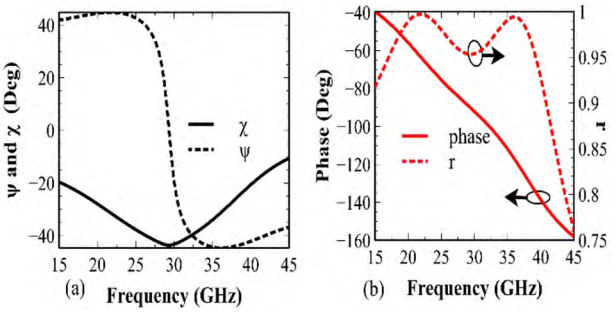

FIGURE 10. (a) The simulated angles of polarization azimuth (ψ) and ellipticity (χ) and (b) the phase difference ($\Delta\phi$) and amplitude ratio (r) versus frequency.

The parameter ψ specifies the angle between the major axis of the ellipse and the x-axis, while the angle χ examines the ellipticity behavior. The angles ψ and χ can be calculated from the following equations [21]:

$$r = \frac{Tr\ (yy)}{Tr\ (xx)} \tag{22}$$

$$\Delta\phi = \varphi_{yy} - \varphi_{xx} \tag{23}$$

$$\psi = \frac{1}{2}(\tan^{-1}\left[\frac{2r}{1-r^2}\right]\cos\Delta\phi) \tag{24}$$

$$\chi = \frac{1}{2}(\sin^{-1}\left[\frac{2r}{1+r^2}\right]\sin\Delta\phi) \tag{25}$$

where "r" in (22) is the amplitude ratio. As shown in Fig. 10 (a), the variations of polarization azimuth angle (ψ) and ellipticity angle (χ) of the transmitted wave with frequency are highlighted. Whenever the ellipticity angle of the transmitted wave is ±45°, it means that polarization is purely circular. Correspondingly, the ellipticity angle of the transmitted wave in the proposed polarizer is −45° at

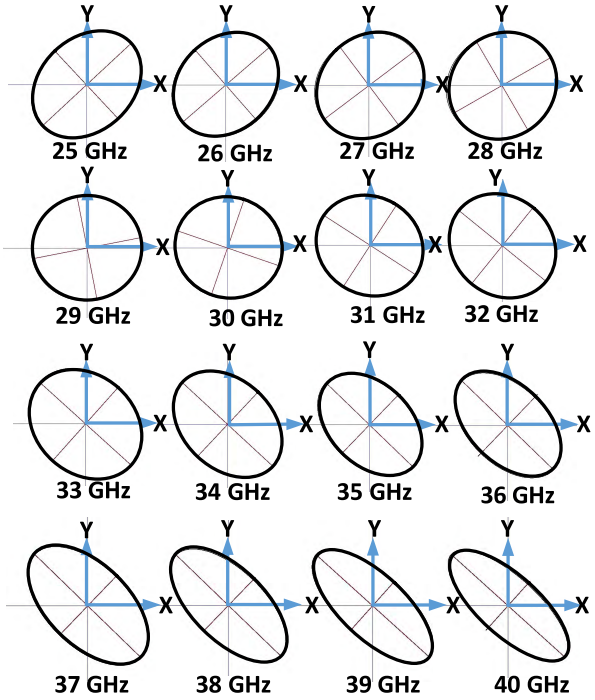

FIGURE 11. Theoretically predicted polarization cases in the plane perpendicular to the wave vector at different frequencies from 25GHz to 40 Ghz.

around 30GHz, indicating the pure CP at the frequencies close to 30GHz, as shown in Fig. 10. To further understand the tendency of the polarization ellipses and its dependence on the frequency, sixteen uniformly distributed frequencies along the bandwidth were selected. The corresponding results are shown in Fig. 11. It can be noticed that by increasing the frequency from 25GHz to 40 GHz, the polarization is right hand rotated. Also, as an acceptable estimation, it is observed that when the ellipticity angle (χ) corresponds to $-45\pm5°$, an excellent CP from 26GHz to 33GHz is obtained. However, an elliptical polarization is observed on the rest of the frequency band. It is expected that the distortions in the circular polarization at the edges of the band are mainly caused by elevated reflections.

Table 1 summarized a brief comparison between the proposed design and sample published polarizers in literature in terms of 3-dB AR bandwidth and maximum insertion loss in the band of interest. According to the table, the proposed design has a better performance compared to other structures, particularly in the insertion loss performance. In order to realize the polarizer performance in practical applications, it is implemented and axial ratio is measured using a wideband horn antenna, as shown in Fig. 12. Fortunately, the measured axial ratio approximately has an acceptable agreement with the simulated one, covering 41% (AR $\leq$ 3dB).

V. INTEGRATED ANTENNA DESIGN

In order to investigate and verify the polarizer performance with an antenna, an 8-element linear array antenna is designed. The wide bandwidth and broadside pattern are two

TABLE 1. Performance comparison of our proposed design with designs in the literature.

Design	3dB AR bandwidth (%)	Peak Insertion loss (dB)
Multilayer based on two-dimensionally anisotropic FSS [5]	40	≤ 3
Meander line and stub [8]	36	1
Cross slot [22]	14.5	3.2
Split circular ring FSS [22]	21	3.3
This work	42	≤ 0.5

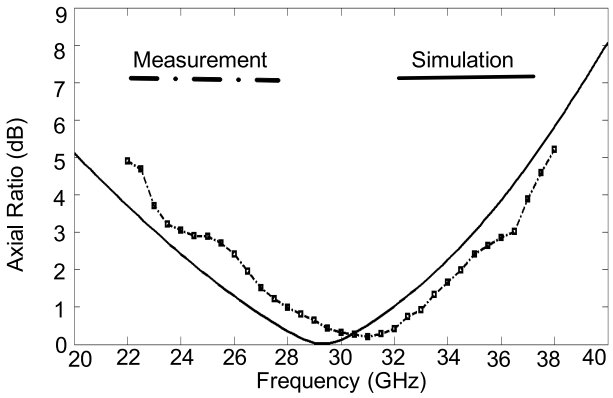

FIGURE 12. The measured and simulated axial ratio of the proposed polarizer with the wideband horn antenna.

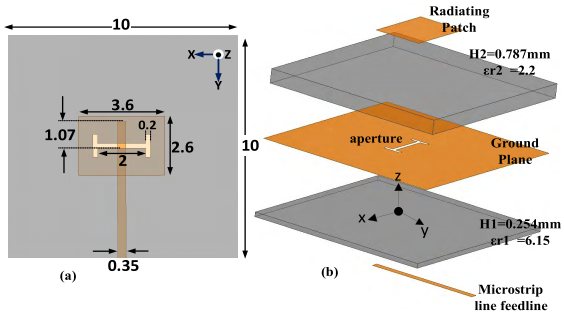

FIGURE 13. The Geometry of the single linear ACMA (a) top view and (b) side view (optimized values are versus millimeter).

main reasons for choosing an aperture-coupled microstrip antenna (ACMA) as the primary prototype. Fig. 13 shows the geometry of a single ACMA feeding operating on Ku-band around 30GHz. The antenna consists of two different substrates, a Rogers RT/Duroid 5880 with dielectric constant 2.2 and thickness 0.787mm on the top and the other is Rogers 3006 with dielectric constant 6.15 and thickness 0.254mm on the bottom. Due to the limitation in the inter-element spacing of linear array structures, an H-shaped slot is etched off the common ground plate [23]. Fig.14 illustrates an equivalent circuit of ACMA similar to the model in [24]. Fig.15, shows the reflection coefficient and total gain of the

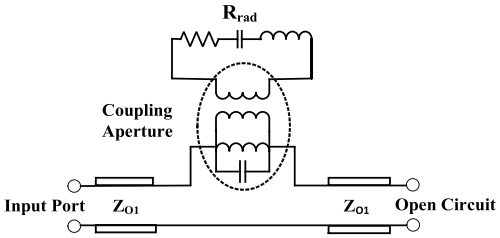

FIGURE 14. The equivalent circuit model of the ACMA [24].

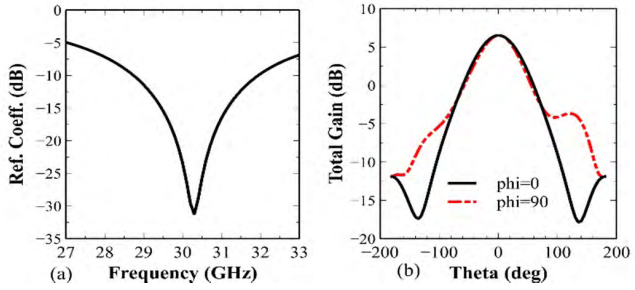

FIGURE 15. (a) The reflection coefficient and (b) radiation pattern of single ACMA at 30GHz.

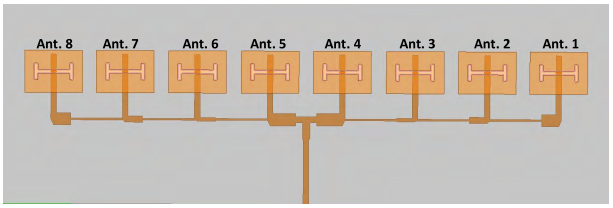

FIGURE 16. The 8-element linearly polarized array ACMA with Chebyshev tapered distribution.

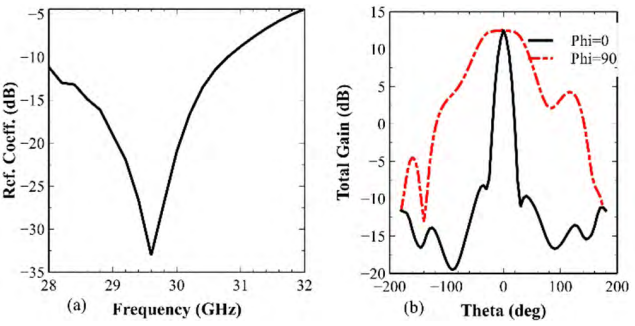

FIGURE 17. (a) The reflection coefficient and (b) radiation pattern of 8-element linear array antennas at 30GHz.

single ACMA. In order to illuminate the transmission-type polarizer, the high gain array antenna with the capability of lower sidelobe level (SLL) is proposed. Thus, an 8-element series-fed linearly polarized array antenna using suitable Chebyshev taper distribution operating at 30GHz is designed. Each antenna element is fed with a 50-ohm input impedance. To design the microstrip series-fed array, firstly the feeding network is divided into two linear subarrays and fed at the center by microstrip line [25].

In order to guarantee the same phase among the elements and to obtain the radiation pattern at broadside, the

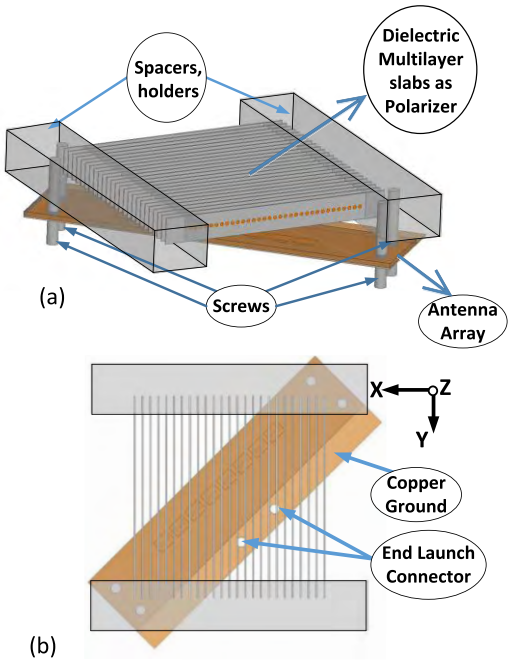

FIGURE 18. The final proposed design, including the multilayer slab polarizer, the antenna array, spacer, screws; (a) side view and (b) top view.

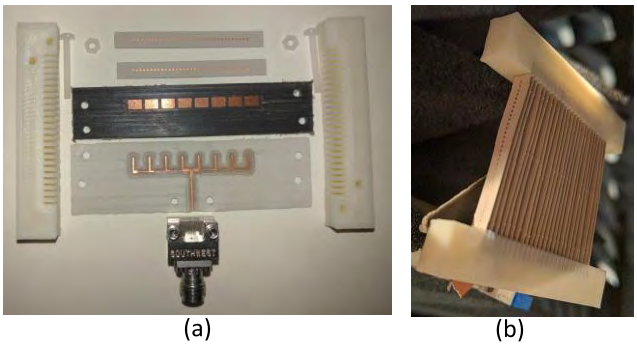

FIGURE 19. The photo of (a) the assembeled design and (b) the propose structure.

distance between the feed points of the array elements has to be equaled to one guided wavelength (λg). The symmetric arrangement reduces the cross-polarization level of the array and minimizes the beam-squinting with frequency [25], [26]. For this case, the cross-polar component produced in one direction of the antenna array is abandoned by the cross-polar component created in the reverse orientation of the antenna array at broadside. Moreover, a tapered distribution is achieved utilizing quarter-wavelength transformers ($\lambda_g/4$) along the line. The simulated reflection coefficient along with radiation pattern on the E-plane and H-plane at 30GHz are shown in Fig. 17. It is observed that the ACMA array resonates at a center frequency close to 30GHz with -23dB H-plane SLL and a gain of 13 dB.

VI. FABRICATION AND EXPERIMENTAL RESULTS

In this section, both the 8-element ACMA LP array and polarizer structures are combined to form the final proposed structure. The LP array is placed under the polarizer using

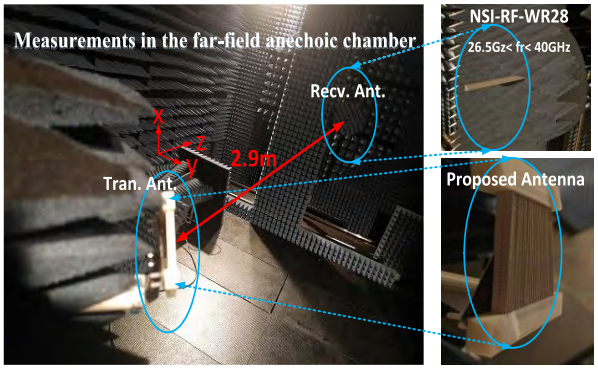

FIGURE 20. The photo of the antenna under test in the far-field anechoic chamber.

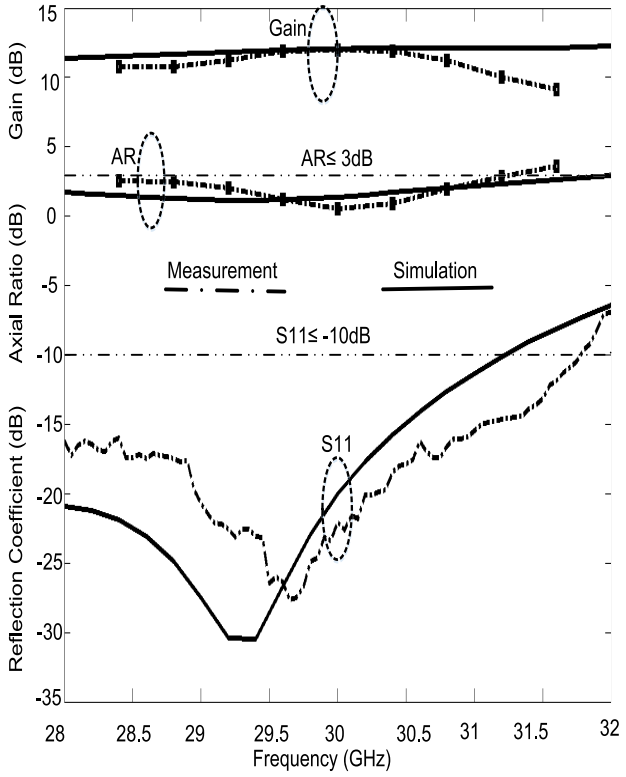

FIGURE 21. The measured and simulated curves of realized gain, axial ratio, and reflection coefficient of the proposed design; including the LP antenna array with the polarizer.

two spacers (holders) with a thickness 5mm (a half wavelength at 30 GHz), as shown in Fig. 18. In order to connect the spacers to the antenna array structure, four screws are used. In addition, an end launch connector from Southwest Company to feed and excite the array is applied. To verify the design and integrated structure's performance, the proposed dielectric multilayer slab polarizer and the 8-element LP-ACMA were fabricated and tested. Fig. 19 shows the photo of the assembled prototype. It consists of two different substrates as the antenna array, dielectric multilayer slabs as the polarizer, spacers, screws, and connector. The measured

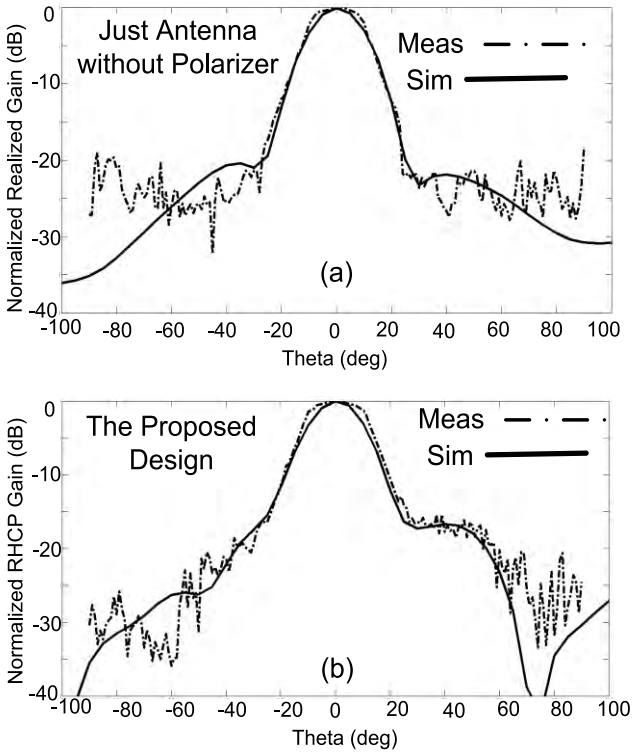

FIGURE 22. (a) The normalized realized gain of the LP antenna array without the polarizer and (b) the normalized RHCP gain of the polarizer with the antenna array at 30GHz.

reflection coefficient of the 8-element linear array ACMA with and without the polarizer were carried out utilizing an Agilent N5227A PNA Network Analyzer (10MHz-67GHz). Also, the far field anechoic chamber is utilized to measure the radiation patterns and axial ratio as depicted in Fig. 20. The left and right-hand electric fields, and AR of the antenna are calculated from the measured electric fields, with both amplitude and phase following [27], [28]:

$$\vec{E}_{RH} = \frac{1}{\sqrt{2}}\left(\vec{E_\theta} + j\vec{E_\emptyset}\right) \tag{26}$$

$$\vec{E}_{LH} = \frac{1}{\sqrt{2}}\left(\vec{E_\theta} - j\vec{E_\emptyset}\right) \tag{27}$$

$$AR(dB) = 10\log\left(\left|\frac{\left|\vec{E}_{RH}\right| + \left|\vec{E}_{LH}\right|}{\left|\vec{E}_{RH}\right| - \left|\vec{E}_{LH}\right|}\right|\right) \tag{28}$$

The measured and simulated results including the reflection coefficient, axial ratio, and realized gain are exhibited in Fig. 21. It can be observed from Fig. 21 that the experimental results and simulated ones have an acceptable agreement. The measured results of the polarizer along with the antenna arary show that impedance bandwidth ($|s11| \leq -10$dB) covers 28GHz to 32GHz with an axial ratio bandwidth (AR$\leq$3dB) from 28GHz to 31.5GHz, and a realized gain of 13dBi with a pure CP at the central frequency of 30GHz. As shown in Fig. 22, the radiation patterns of the proposed antenna array with and without the polarizer at 30GHz are presented.

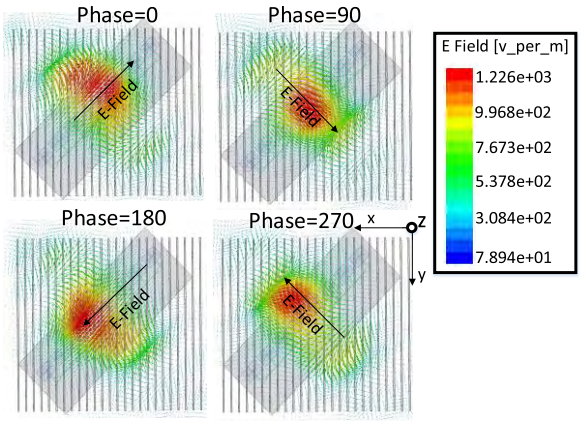

FIGURE 23. (a) RHCP far E-field variations at different phases (a) 0°, (b) 90°, (c) 180°, and (d) 270° at the centre frequency 30 GHz.

From the normalized realized gain curve in Fig. 22(a), it can be observed that the sidelobe level (SLL) is nearly −20dB due to the Chebyshev tapered distribution used in the feed line. Fig. 22 (b) shows the normalized RHCP gain of the final proposed integrated structure including both the antenna array and polarizer.

The simulated and measured results have an acceptable agreement in the main beam angular region. In Fig. 23, it can be realized that the radiated field from the antenna rotates in clockwise direction demonstrating a right-hand circularly polarized wave.

VII. CONCLUSION

In this paper, a new polarizer based on dielectric multilayer slabs for MMW applications is presented. The polarizer can function from 23 GHz to 35 GHz (42%) with excellent impedance and AR bandwidths. The insertion loss of polarizer is less than 0.5 dB which in industrial applications can be excellent. The polarizer is fabricated and measured by a wideband horn antenna satisfying the simulated results. Next, in order to design a high-gain circularly polarized structure at around 30 GHz, an 8-element LP array antenna with Chebyshev tapered distribution is designed and integrated with the polarizer. Obviously, the antenna retricts the overall bandwidth due to the narrowband nature of the LP antenna array. The combined structure was fabricated and measured. There is an excellent agreement between the experimental results with the simulated ones. The measured results of the fabricated structure show that the final design is able to cover impedance and axial-ratio bandwidths nearly 28 GHz to 31.5 GHz. Furthermore, it has a pure CP and realized a gain of 13 dBi at 30 GHz. This polarizer with the antenna array can be a suitable candidate for several applications including satellite communications, orthogonal polarization transformers, sub-reflectors, and CP lenses.

ACKNOWLEDGMENT

The authors would like to thank S. Zarbakhsh of Concordia University, Canada, for his invaluable contributions.

REFERENCES

[1] M. Akbari, H. A. Ghalyon, M. Farahani, A.-R. Sebak, and T. A. Denidni, "Spatially decoupling of CP antennas based on FSS for 30-GHz MIMO systems," *IEEE Access*, vol. 5, pp. 6527–6537, May 2017.
[2] M. Akbari, S. Gupta, M. Farahani, A. R. Sebak, and T. A. Denidni, "Gain enhancement of circularly polarized dielectric resonator antenna based on FSS superstrate for MMW applications," *IEEE Trans. Antennas Propag.*, vol. 64, no. 12, pp. 5542–5546, Dec. 2016.
[3] M. Akbari, S. Gupta, M. Farahani, A. R. Sebak, and T. A. Denidni, "Analytic study on CP enhancement of millimeter wave DR and patch subarray antennas," *Int. J. RF Microw. Comput.-Aided Eng.*, vol. 27, no. 1, p. e21053, Jan. 2017.
[4] L. Li, Y. Li, Z. Wu, F. Huo, Y. Zhang, and C. Zhao, "Novel polarization-reconfigurable converter based on multilayer frequency-selective surfaces," *Proc. IEEE*, vol. 103, no. 7, pp. 1057–1070, Jul. 2015.
[5] S. M. A. M. H. Abadi and N. Behdad, "Wideband linear-to-circular polarization converters based on miniaturized-element frequency selective surfaces," *IEEE Trans. Antennas Propag.*, vol. 64, no. 2, pp. 525–534, Feb. 2016.
[6] R. Orr, G. Goussetis, and V. Fusco, "Design method for circularly polarized Fabry–Perot cavity antennas," *IEEE Trans. Antennas Propag.*, vol. 62, no. 1, pp. 19–26, Jan. 2014.
[7] L. Martinez-Lopez, J. Rodriguez-Cuevas, J. I. Martinez-Lopez, and A. E. Martynyuk, "A multilayer circular polarizer based on bisected split-ring frequency selective surfaces," *IEEE Antennas Wireless Propag. Lett.*, vol. 13, pp. 153–156, Jan. 2014.
[8] M.-A. Joyal and J.-J. Laurin, "Analysis and design of thin circular polarizers based on meander lines," *IEEE Trans. Antennas Propag.*, vol. 60, no. 6, pp. 3007–3011, Jun. 2012.
[9] P. Fei, Z. Shen, X. Wen, and F. Nian, "A single-layer circular polarizer based on hybrid meander line and loop configuration," *IEEE Trans. Antennas Propag.*, vol. 63, no. 10, pp. 4609–4614, Oct. 2015.
[10] J. M. I. Alonso, G. A. Calderón, and M. S. Pérez, "SIW antenna with polarizer at ku-band," *IEEE Trans. Antennas Propag.*, vol. 63, no. 6, pp. 2782–2786, Jun. 2015.
[11] X.-C. Zhu *et al.*, "Design of a bandwidth-enhanced polarization rotating frequency selective surface," *IEEE Trans. Antennas Propag.*, vol. 62, no. 2, pp. 940–944, Feb. 2014.
[12] H. L. Zhu, S. W. Cheung, K. L. Chung, and T. I. Yuk, "Linear-to-circular polarization conversion using metasurface," *IEEE Trans. Antennas Propag.*, vol. 61, no. 9, pp. 4615–4623, Sep. 2013.
[13] Y. Cheng, C. Wu, Z. Z. Cheng, and R. Z. Gong, "Ultra-compact multi-band chiral metamaterial circular polarizer based on triple twisted split-ring resonator," *Prog. Electromagn. Res.*, vol. 155, pp. 105–113, Mar. 2016.
[14] M. Mutlu, A. E. Akosman, and E. Ozbay, "Broadband circular polarizer based on high-contrast gratings," *Opt. Lett.*, vol. 37, no. 11, pp. 2094–2096, 2012.
[15] J. D. Jackson, *Classical Electrodynamics*, 3rd ed. Hoboken, NJ, USA: Wiley, 1999, pp. 205–207.
[16] C. A. Balanis, *Antenna Theory Analysis and Design*, 2nd ed. Hoboken, NJ, USA: Wiley, 1997.
[17] B. Li and Z. Shen, "Three-dimensional bandpass frequency-selective structures with multiple transmission zeros," *IEEE Trans. Microw. Theory Techn.*, vol. 61, no. 10, pp. 3578–3589, Oct. 2013.
[18] A. K. Rashid and B. L. Z. Shen, "An overview of three-dimensional frequency-selective structures," *IEEE Antennas Propag. Mag.*, vol. 56, no. 3, pp. 43–67, Jun. 2014.
[19] J. D. Shumpert, "Modeling of periodic dielectric structures (electomagnetic crystals)," Ph.D. dissertation, Dept. Elect. Eng., Univ. Michigan, Ann Arbor, MI, USA, 2001.
[20] R. E. Collin, *Foundations for Microwave Engineering*. New York, NY, USA: McGraw-Hill, 1992.
[21] Z. Li, W. Liu, H. Cheng, S. Chen, and J. Tian, "Realizing broadband and invertible linear-to-circular polarization converter with ultrathin single-layer metasurface," *Sci. Rep.*, vol. 5, Dec. 2015, Art. no. 18106.
[22] M. Euler, V. Fusco, R. Dickie, R. Cahill, and J. Verheggen, "Sub-mm wet etched linear to circular polarization FSS based polarization converters," *IEEE Trans. Antennas Propag.*, vol. 59, no. 8, pp. 3103–3106, Aug. 2011.
[23] S.-C. Gao, L.-W. Li, M.-S. Leong, and T.-S. Yeo, "Wide-band microstrip antenna with an H-shaped coupling aperture," *IEEE Trans. Veh. Technol.*, vol. 51, no. 1, pp. 17–27, Jan. 2002.
[24] A. Pirhadi, H. Bahrami, and J. Nasri, "Wideband high directive aperture coupled microstrip antenna design by using a FSS superstrate layer," *IEEE Trans. Antennas Propag.*, vol. 60, no. 4, pp. 2101–2106, Apr. 2012.

[25] R. Bayderkhani and H. R. Hassani, "Wideband and low sidelobe slot antenna fed by series-fed printed array," *IEEE Trans. Antennas Propag.*, vol. 58, no. 12, pp. 3898–3904, Dec. 2010.
[26] M. Farahani, J. Pourahmadazar, M. Akbari, M. Akbari, A. R. Sebak, and T. A. Denidni, "Mutual coupling reduction in millimeter-wave MIMO antenna array using a metamaterial polarization-rotator wall," *IEEE Antennas Wireless Propag. Lett.*, vol. 16, pp. 2324–2327, 2017.
[27] S. L. S. Yang, R. Chair, A. A. Kishk, K. F. Lee, and K. M. Luk, "Study on sequential feeding networks for subarrays of circularly polarized elliptical dielectric resonator antenna," *IEEE Trans. Antennas Propag.*, vol. 55, no. 2, pp. 321–333, Feb. 2007.
[28] S. Vakilinia, B. Heidarpour, and M. Cheriet, "Energy efficient resource allocation in cloud computing environments," *IEEE Access*, vol. 4, pp. 8544–8557, 2016.
[29] S. Yan and G. A. E. Vandenbosch, "Compact circular polarizer based on chiral twisted double split-ring resonator," *Appl. Phys. Lett.*, vol. 102, no. 10, p. 103503, Mar. 2013.

MOHAMMAD AKBARI (S'15) received the B.Sc. degree in telecommunication engineering from the University of Shahid Bahonar, Kerman, Iran, in 2007, and the M.Sc. degree in electrical engineering–telecommunication from the University of Urmia, Urmia, Iran, in 2011. He is currently pursuing the Ph.D. degree with Concordia University, Montreal, Canada. He has taught courses in microwave engineering, antenna theory, and fields & waves, and electromagnetic as an Instructor. He has authored or co-authored over 60 peer-reviewed scientific journals and international conference papers. His research interests include the analysis and design of periodic structures, such as FSS and EBG for different applications, such as polarizer, RCS reduction, coupling suppression, gain enhancement, the design of flexible electronics, wearable antennas, textile antennas for RFID and wireless communication systems, antenna integration and miniaturization techniques, electrically small antennas, reconfigurable antennas, cognitive radio systems, ultrawideband technology and communication systems, the modeling of microwave structures, metamaterial-inspired antennas, dispersion engineering, miniaturization techniques, reconfigurable antennas, antenna interactions with human body, mm-wave technology, phased and switched-beam arrays, microstrip antennas and circuits, and sequential feedings. He received the Graduate Concordia Merit Scholarship and the Tuition Fee Remission Award.

MOHAMMADMAHDI FARAHANI (S'16) received the Diploma degree in electrical engineering, applied electromagnetisms engineering, from the Iran University of Science and Technology (IUST), Tehran, Iran, in 2012. He is currently pursuing the Ph.D. degree with the Institut National de la Recherche Scientifique, Universite de Quebec, Montreal, QC, Canada. He was a Researcher with the IUST Antennas & Microwave Research Laboratory with the RF Communications Systems Group, from 2009 to 2012. His current research interests include phase array antennas, adaptive arrays, switched multibeam antenna arrays, FSS structures, dielectric resonator antennas, metamaterial antennas, and microwave components development for wireless communications systems.

ABDEL-RAZIK SEBAK (F'10) received the B.Sc. degree (Hons.) in electrical engineering from Cairo University, Cairo, Egypt, in 1976, the B.Sc. degree in applied mathematics from Ein Shams University, Cairo, in 1978, and the M.Eng. and Ph.D. degrees in electrical engineering from the University of Manitoba, Winnipeg, MB, Canada, in 1982 and 1984, respectively. From 1984 to 1986, he was with Canadian Marconi Company involving in the design of microstrip phased array antennas. From 1987 to 2002, he was a Professor with the Department of Electronics and Communication Engineering, University of Manitoba. He is currently a Professor with the Department of Electrical and Computer Engineering, Concordia University, Montreal, QC, Canada. His research interests include phased array antennas, millimeter-wave antennas and imaging, computational electromagnetics, and interaction of EM waves with engineered materials and bio electromagnetics. He is a member of the Canadian National Committee of International Union of Radio Science Commission B. He was a recipient of the 2000 and 1992 University of Manitoba Merit Award for outstanding Teaching and Research, the 1994 Rh Award for Outstanding Contributions to Scholarship and Research, and the 1996 Faculty of Engineering Superior. He has served as the Chair of the IEEE Canada Awards and Recognition Committee from 2002 to 2004, and as the Technical Program Chair of the 2002 IEEE CCECE Conference and the 2006 URSIANTEM Symposium. He is the Technical Program Co-Chair for the 2015 IEEE ICUWB Conference.

TAYEB A. DENIDNI (M'98–SM'04) received the M.Sc. and Ph.D. degrees in electrical engineering from Laval University, Quebec, QC, Canada, in 1990 and 1994, respectively. He was a Professor with the Engineering Department, Université du Quebec in Rimouski, Rimouski, QC, Canada, from 1994 to 2000, where he founded the Telecommunications Laboratory. Since 2000, he has been with the Institut National de la Recherche Scientifique (INRS), Université du Quebec, Montreal, QC, Canada. He found the RF Laboratory with INRS-EM. He has extensive experience in antenna design. He is leading a Large Research Group consisting of three research scientists, eight Ph.D. students, and two M.Sc. students. His current research interests include reconfigurable antennas using EBG and FSS structures, dielectric resonator antennas, metamaterial antennas, adaptive arrays, switched multi-beam antenna arrays, ultrawideband antennas, microwave, and development for wireless communications systems. He served as an Associate Editor of the IEEE TRANSACTIONS ON ANTENNAS AND PROPAGATION from 2008 to 2010. From 2005 to 2007, he served as an Associate Editor of the IEEE ANTENNAS WIRELESS PROPAGATION LETTERS. Since 2015, he has been an Associate Editor of the *IET Electronics Letters*.